

# Topological Edge and Corner States in Biphenylene Photonic Crystal

HUYEN THANH PHAN,<sup>1,\*</sup> KEIKI KOIZUMI,<sup>1</sup> FENG LIU,<sup>2,3,†</sup> AND KATSUNORI WAKABAYASHI<sup>1,4,5,‡</sup>

<sup>1</sup>*Department of Nanotechnology for Sustainable Energy, School of Science and Technology, Kwansai Gakuin University, Gakuen-Uegahara 1, Sanda, Hyogo 669-1330, Japan*

<sup>2</sup>*School of Physical Science and Technology, Ningbo University, Ningbo 315-211, China*

<sup>3</sup>*Institute of High Pressure Physics, Ningbo University, Ningbo 315-211, China*

<sup>4</sup>*Center for Spintronics Research Network (CSRN), Osaka University, Toyonaka 560-8531, Japan*

<sup>5</sup>*National Institute for Materials Science (NIMS), Tsukuba, Ibaraki 305-0044, Japan*

\*[phanthanhhuyenpth@gmail.com](mailto:phanthanhhuyenpth@gmail.com)

†[liufeng@nbu.edu.cn](mailto:liufeng@nbu.edu.cn)

‡[waka@kwansai.ac.jp](mailto:waka@kwansai.ac.jp)

**Abstract:** The biphenylene network (BPN) has a unique two-dimensional atomic structure, where hexagonal unit cells are arranged on a square lattice. Inspired by such a BPN structure, we design a counterpart in the fashion of photonic crystals (PhCs), which we refer to as the BPN PhC. We study the photonic band structure using the finite element method and characterize the topological properties of the BPN PhC through the use of the Wilson loop. Our findings reveal the emergence of topological edge states in the BPN PhC, specifically in the zigzag edge and the chiral edge, as a consequence of the nontrivial Zak phase in the corresponding directions. In addition, we find the localization of electromagnetic waves at the corners formed by the chiral edges, which can be considered as second-order topological states, i.e., topological corner states.

## 1. Introduction

Topology originates from mathematics, which helps distinguish the geometric structure by invariant quantities during continuous deformation. For example, a closed surface is classified by the number of hole in it. This number remains unchanged without cutting the surface. When topology is applied to physics [1–4], some novel properties are found to be robust to perturbations and have potential applications in the realization of disorder-free spin transport [5–12]. One of the most important features on nontrivial topological systems is the emergence of edge states [13–17]. These topologically protected edge states are characterized by the nontrivial energy band inversions at high symmetric points and become a strong candidate for further study of quantum computation. Moreover, recent studies of higher-order topology have extended these topological edge states to the corner states in two-dimensional (2D) systems [18–21]. This research direction becomes increasingly attractive because of its potential applications. For example, quantum computation can be designed based on topological corner states [22–26].

By applying topology to photonic crystalline systems, the photonic analogy of the quantum Hall effect was theoretically proposed by Raghu and Haldane [27, 28], then experimentally observed in 2D photonic crystals (PhCs) [29, 30]. These seminal works have stimulated many other investigations on the topological edge states of PhCs [31–35]. After that, researchers have become more and more interested in the studies of topological PhCs. The photonic analogy of Chern insulators is also found due to non-zero Berry curvature in broken time-reversal symmetry [29, 36, 37]. In addition, even in the zero Berry curvature, topological states can emerge in the PhC systems [38–40]. These states are explained by nontrivial Zak phase [41, 42], gapped Wannier bands [43–47] and valleys interaction [48].

Designing a topologically nontrivial PhC usually requires the breaking of discrete particle

symmetry, such as the time-reversal symmetry, which is not easy to achieve. Another routine is to mimic the existing structures in electronic materials such as graphene [10, 17, 49]. Following the successful applications of graphene and other nanoelectronic materials, the search for 2D carbon allotropes other than graphene, such as biphenylene network (BPN) or graphenylene network, has stimulated and brought a new insight into electronic transport properties in nanoscale materials. Especially, BPN has a fascinating lattice structure, where the hexagonal unit cells are organized on a square lattice, resulting in a two-dimensional tiling pattern that includes four-, six-, and eight-membered rings [50, 51]. Motivated by recent experimental development of the BPN sheet, we design a PhC that has an atomic structure and arrangement similar to those of the BPN and focus on its topological properties such as the emergence of topological edge and corner states. In this work, we use the finite element method to evaluate the photonic band structures of BPN PhC and utilize the Wilson loop to analyze their topological properties. We find several different ribbon structures induce the topological edge states which are attributed to the presence of a nontrivial Zak phase. Furthermore, when the product of the Zak phases for two edge structures forming a corner is non-zero, it results in the appearance of second-order topological states [40, 52, 53]. These results suggest potential applications of topological edge and corner states in PhC devices.

The paper is organized as follows. In Section 2, we introduce BPN PhC structure and numerically calculate the photonic band structure. Section 3 is used to evaluate the Zak phase and discuss the existence of topological edge states. The second-order topology as corner states is presented in Section 4. We discuss the results and summarize the paper in Section 5.

## 2. Biphenylene Photonic Crystal

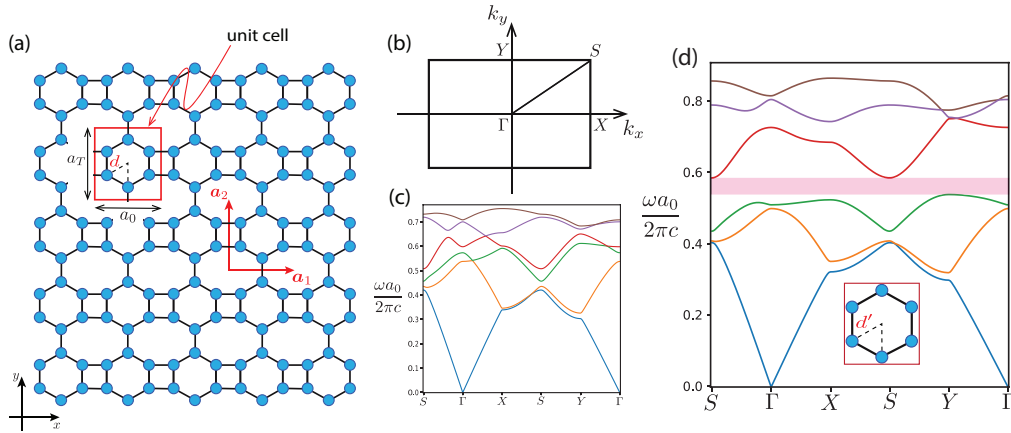


Fig. 1. (a) Schematic of 2D BPN PhC. The red rectangle indicates the primitive unit cell, which contains six equivalent dielectric rods, colored by cyan. The radius of these rods is  $r_0$ , and the distance between each rod and the center of the unit cell is  $d$ .  $\mathbf{a}_1 = (a_0, 0)$  and  $\mathbf{a}_2 = (0, a_T)$  are primitive lattice vectors. Here,  $a_0$  and  $a_T \equiv 3a_0/(\sqrt{3} + 1)$  are the lattice periodicity in the  $x$ - and  $y$ -directions, respectively. (b) 1st BZ of the 2D BPN lattice. (c) Photonic band structure of 2D BPN PhC for  $d = a_T/3$ ,  $r_0 = 0.2d$ . (d) Photonic band structure for the modified BPN PhC where  $d' = 1.3a_T/3$ ,  $r_0 = 0.2d$ . The inset shows the schematic of one unit cell of modified BPN PhC.

Here we introduce BPN PhC and calculate its photonic band structure. Figure 1(a) shows the lattice structure of BPN PhC, where the red rectangle indicates the primitive unit cell. There

are six equivalent dielectric rods in one unit cell, colored by cyan. Radius for each rod is  $r_0$ . In this paper, we assume that the dielectric rods are all made of silicon, with a dielectric constant of  $\varepsilon = 11.7$ . These rods are arranged periodically in form of the BPN lattice, where the lattice periodicity in  $x$ - and  $y$ -directions are  $a_0$  and  $a_T = 3a_0/(\sqrt{3} + 1)$ , respectively. The primitive vectors of BPN PhC are  $\mathbf{a}_1 = (a_0, 0)$  and  $\mathbf{a}_2 = (0, a_T)$ . The distance between the two nearest dielectric rods is  $d$ , which is equal to the distance between each rod and the center of the unit cell. We focus on the transverse magnetic modes of the electromagnetic (EM) waves so that the magnetic field is in the  $xy$  plane, the electric field is perpendicular to the  $xy$  plane. Assuming the harmonic oscillation in time dependence, the eigenvalue equation of the PhC is given as

$$\frac{1}{\varepsilon(\mathbf{r})} \nabla \times \nabla \times \mathbf{E}(\mathbf{r}) = \frac{\omega^2}{c^2} \mathbf{E}(\mathbf{r}), \quad (1)$$

where  $\mathbf{E}(\mathbf{r})$  is the electric field and  $\varepsilon(\mathbf{r})$  is dielectric function.  $\mathbf{r} = (x, y)$  is the position vector in 2D space.  $c$  is the speed of light in vacuum.  $\omega$  is the eigenfrequency. Figure 1(b) shows the corresponding 1st Brillouin zone (BZ) for 2D BPN lattice with high symmetric points.

The photonic band structure for  $d = a_T/3$  and  $r_0 = 0.2d$  are shown in Fig. 1(c). As can be seen, there is no band gap in this PhC structure, all bands connect to others by linear dispersion at degenerate points. To examine the topological properties of BPN PhC, we need to open a complete band gap in the photonic band structure. Therefore, we slightly modify the lattice structure by increasing the distance  $d$  between each rod and the center of the unit cell, i.e.  $d' = 1.3d$ . The radii of all rods and the size of the unit cell remain the same as the original structure, which can be seen in the inset of Fig. 1(d).

The modified photonic band structure is shown in Fig. 1(d). A complete band gap, labeled by shaded pink color, is found around the normalized frequency 0.55 and is between the 3rd and the 4th band. The 1st and the 2nd photonic bands are still connected by a degenerate point along the  $S - Y$  line. The 3rd band is now isolated from the others with small photonic band gap. For simplicity, we will examine the modified BPN PhC and focus on the three lowest photonic bands below the band gap.

### 3. Zak Phase and Topological Edge States

In this section, we elaborate the numerical calculation method used to evaluate the Zak phase. Then, we discuss the localization of EM waves at the edges for several ribbon structures.

The Zak phase is commonly calculated for one-dimensional (1D) periodic systems. It is mathematically defined as the 1D integration of the Berry connection over the 1st BZ [54]. Since this integration occurs along a single dimension, the Zak phase of 2D periodic systems depends on the other direction that is perpendicular to the integration line [13], which can also be considered as a Wilson loop. For instance, within the 1st BZ of a 2D square lattice, the Zak phase along the  $k_x$  direction should be determined by integrating the Berry connection along the  $k_y$  direction.

To evaluate numerically the Zak phase of BPN edges with several different edge structures, we shall briefly illustrate the lattice structure of BPN ribbons and their relevant structural parameters. In Fig. 2(a), we present three typical edge structures of BPN ribbons, which are referred as zigzag, armchair and chiral edges. These are indicated by red, green and blue lines, respectively. For zigzag edges, the lattice is translational invariant under the translational vector  $\mathbf{T} = \mathbf{a}_1$ . Similarly, for armchair edges, the translational vector is  $\mathbf{T} = \mathbf{a}_2$ , and for chiral edges,  $\mathbf{T} = \mathbf{a}_1 + \mathbf{a}_2$ .

In general, we assume that the translational vector of BPN edges can be defined as  $\mathbf{T} = m\mathbf{a}_1 + n\mathbf{a}_2$ , where  $\mathbf{a}_1$  and  $\mathbf{a}_2$  are two primitive lattice vectors,  $m$  and  $n$  are coprime integers. If they are not coprime, the two vectors defined below do not form the basis set in reciprocal space. Normally, the 2D momentum area that is used to calculate the Zak phase is the 1st BZ. In more a

general case, that 2D momentum area is chosen as a rectangular area formed by two orthogonal vectors  $\Gamma_{\parallel}$  and  $\Gamma_{\perp}$ . These two vectors are defined as follows

$$\Gamma_{\parallel} = 2\pi \frac{\mathbf{T}}{|\mathbf{T}|^2}. \quad (2)$$

$\Gamma_{\parallel}$  is parallel to the edge orientation (parallel to  $\mathbf{T}$ ). Thus, the 1st BZ for BPN edges can be defined as  $-\frac{\pi}{|\mathbf{T}|} \leq k \leq \frac{\pi}{|\mathbf{T}|}$ . The 2nd vector  $\Gamma_{\perp}$  is perpendicular to  $\Gamma_{\parallel}$  and relates to  $\Gamma_{\parallel}$  by the following formula

$$\Gamma_{\parallel} \times \Gamma_{\perp} = \mathbf{b}_1 \times \mathbf{b}_2, \quad (3)$$

where  $\mathbf{b}_1$  and  $\mathbf{b}_2$  are two primitive vectors in reciprocal space and defined by  $\mathbf{a}_i \cdot \mathbf{b}_j = 2\pi\delta_{ij}$  ( $i, j = 1, 2$ ). Equation (3) indicates that the area of the new momentum area formed by  $\Gamma_{\parallel}$  and  $\Gamma_{\perp}$  is equal to the area of the original 1st BZ. All the translational and reciprocal vectors for zigzag, armchair and chiral edges are summarized in Table 1.

Table 1. **Translational and reciprocal vectors for zigzag, armchair and chiral edges.**

Edge Structure	$\mathbf{T}$	$\Gamma_{\parallel}$	$\Gamma_{\perp}$
Zigzag	$\mathbf{a}_1$	$\begin{pmatrix} \frac{2\pi}{a_0} \\ 0 \end{pmatrix}$	$\begin{pmatrix} 0 \\ \frac{2\pi}{a_T} \end{pmatrix}$
Armchair	$\mathbf{a}_1$	$\begin{pmatrix} 0 \\ \frac{2\pi}{a_T} \end{pmatrix}$	$\begin{pmatrix} \frac{2\pi}{a_0} \\ 0 \end{pmatrix}$
Chiral	$\mathbf{a}_1 + \mathbf{a}_2$	$\frac{2\pi}{a_0} \begin{pmatrix} 4 + 2\sqrt{3} & 3 + 3\sqrt{3} \\ 13 + 2\sqrt{3} & 13 + 2\sqrt{3} \end{pmatrix}$	$\frac{2\pi}{a_0} \begin{pmatrix} 1 \\ -\frac{1 + \sqrt{3}}{3} \end{pmatrix}$

In Fig. 2(b), we display the momentum areas, which are used to calculate the Zak phase. The blue rectangle is the momentum area used for calculating the Zak phase of the zigzag and armchair edges, which is completely overlapped with the 1st BZ of bulk 2D BPN. The red and green bold lines are the 1st BZ for zigzag and armchair edges, respectively. The orange rectangle is the momentum area for computing the Zak phase of the chiral edge, the blue bold line denotes the 1st BZ for chiral edges. The size of each momentum area is expressed as the black text in the figure.

The electric field propagating in the PhCs can be written in term of Bloch wave function as  $\mathbf{E}_{\mathbf{k}}^n(\mathbf{r}) = \mathbf{u}_{\mathbf{k}}^n(\mathbf{r}) e^{i\mathbf{k}\mathbf{r}}$ , where  $\mathbf{u}_{\mathbf{k}}^n(\mathbf{r})$  is the periodic function with the same periodicity as the PhCs. Before calculating the Zak phase, we define the scalar product of two periodic functions as

$$\langle \mathbf{u}_{\mathbf{k}}^n | \mathbf{u}_{\mathbf{k}'}^n \rangle = \int_{\text{unit cell}} \mathbf{u}_{\mathbf{k}}^n(\mathbf{r})^* \mathbf{u}_{\mathbf{k}'}^n(\mathbf{r}) d\mathbf{r}, \quad (4)$$

For the edge in any direction characterized by vector  $\mathbf{T}$ , the Zak phase of the  $n$ -th band is computed by integrating the Berry connection over  $\Gamma_{\perp}$  as

$$Z^n(k_{\parallel}) = \oint_{\Gamma_{\perp}} \langle \mathbf{u}_{\mathbf{k}}^n | i\partial_{\mathbf{k}} | \mathbf{u}_{\mathbf{k}}^n \rangle dk_{\perp}, \quad (5)$$

where  $k_{\parallel}$  and  $k_{\perp}$  are  $k$ -points in  $\Gamma_{\parallel}$  and  $\Gamma_{\perp}$  directions, respectively. For numerical calculation, we make an approximation for Eq. (5) by dividing  $\Gamma_{\parallel}$  and  $\Gamma_{\perp}$  into  $N_0$  segments then taking the sum of the contribution of each segment. We obtain the discrete formula similar to the Wilson loop as shown below

$$Z^n(k_i) = -\text{Im} \left( \log \prod_{k_j} \langle \mathbf{u}_{k_i, k_j}^n | \mathbf{u}_{k_i, k_{j+1}}^n \rangle \right), \quad (6)$$

where  $k_i$  is discrete  $k$ -point of  $\Gamma_{\parallel}$  and  $k_j$  is discrete  $k$ -point of  $\Gamma_{\perp}$ , ( $i, j = 1, \dots, N_0$ ). The Eq. (6) indicates that the Zak phase can be calculated for each  $k_i$  point in the  $\Gamma_{\parallel}$  direction. Equation (6) is used for a single band. For a group of degenerate bands, the scalar products are replaced by overlap matrices [37, 55]. The overlap matrix  $S$  for the group of  $N$  degenerate bands between two  $k$ -point  $\mathbf{k}_1$  and  $\mathbf{k}_2$  is

$$S_{\mathbf{k}_1\mathbf{k}_2} = \begin{bmatrix} \langle \mathbf{u}_{\mathbf{k}_1}^1 | \mathbf{u}_{\mathbf{k}_2}^1 \rangle & \langle \mathbf{u}_{\mathbf{k}_1}^1 | \mathbf{u}_{\mathbf{k}_2}^2 \rangle & \dots & \langle \mathbf{u}_{\mathbf{k}_1}^1 | \mathbf{u}_{\mathbf{k}_2}^N \rangle \\ \langle \mathbf{u}_{\mathbf{k}_1}^2 | \mathbf{u}_{\mathbf{k}_2}^1 \rangle & \langle \mathbf{u}_{\mathbf{k}_1}^2 | \mathbf{u}_{\mathbf{k}_2}^2 \rangle & \dots & \langle \mathbf{u}_{\mathbf{k}_1}^2 | \mathbf{u}_{\mathbf{k}_2}^N \rangle \\ \dots & \dots & \dots & \dots \\ \langle \mathbf{u}_{\mathbf{k}_1}^N | \mathbf{u}_{\mathbf{k}_2}^1 \rangle & \langle \mathbf{u}_{\mathbf{k}_1}^N | \mathbf{u}_{\mathbf{k}_2}^2 \rangle & \dots & \langle \mathbf{u}_{\mathbf{k}_1}^N | \mathbf{u}_{\mathbf{k}_2}^N \rangle \end{bmatrix}, \quad (7)$$

where the index  $l$  of  $\mathbf{u}_{\mathbf{k}}^l$  indicates band index.

Take the summation product over the period along the  $k_j$ , we obtain the Wilson-loop-like matrix as

$$\hat{S}(k_i) = \prod_{k_j} S_{k_i k_j, k_i k_{j+1}}, \quad (8)$$

The Zak phase for  $n$ -th band can be then solved by the  $n$ -th eigenvalues  $s^n$  of the Wilson loop matrix  $\hat{S}(k_i)$ . The Zak phase for  $n$ -th subband is given by

$$Z^n(k_i) = -\text{Im} \log(s^n). \quad (9)$$

As can be seen in photonic band structure in Fig. 1(d), the 1st and the 2nd photonic bands are entangled with a degenerate point, however, the 3rd photonic band is isolated. To calculate the Zak phase for each type of edge, we use Eq. (9) for the entangled 1st and 2nd photonic bands, Eq. (6) for the isolated 3rd photonic band, respectively.

Here we shall evaluate the Zak phase of BPN ribbon with zigzag edges and observe the emergence of topological edge states in photonic band structure, which are associated with the nonzero Zak phase. Figure 3(a) is a schematic of the zigzag ribbon, which is periodic along the  $x$ -direction and its width in the  $y$ -direction is  $20a_T$ . In our numerical calculations, we use the following boundary conditions: periodic boundary condition (PBC) for  $x$ -direction, and perfect magnetic conductor (PMC) boundary condition for  $y$ -direction, respectively. Figure 3(b) shows the numerically obtained Zak phase for the lowest three photonic bands. Figure 3(c) shows the numerically obtained photonic bands for BPN ribbon with zigzag edges, where the red lines indicate the modes owing to topological edge states.

As shown in Fig. 3(b), the 1st and the 2nd photonic bands have  $k$ -dependent Zak phase owing to the band inversion at the degenerate point along the  $S - Y$  line in the 1st BZ of bulk 2D BPN. The total Zak phase for lowest two bands is  $\sum_{n=1}^2 Z^n(k) = \pi$ , which should lead to the topological edge states between the 2nd and the 3rd photonic bands for all  $k$  points. However, since the band gap between the 2nd and the 3rd photonic bands is not a complete band gap in the present system, the edge states near  $k = 0$  are mixed with bulk states that cannot be detected by numerical calculation. Similarly, since the total Zak phase for the lowest three bands is  $\sum_{n=1}^3 Z^n(k) = \pi$ , the edge states are expected to emerge for all over  $k$  between the 3rd and the 4th photonic bands. However, it emerges only at the center of the 1st BZ because of the PMC boundary condition. To realize the topological edge states in the whole 1st BZ, we need to change the boundary condition by creating the interface between the zigzag edge and a trivial PhC, which will be shown later.

Next we shall discuss the case for BPN ribbon with armchair edges. Figure 3(d) is the schematic of BPN ribbon with armchair edges. Since the system is only periodic along  $y$ -direction and its width in the  $x$ -direction is  $20a_0$ , we shall impose the following boundary

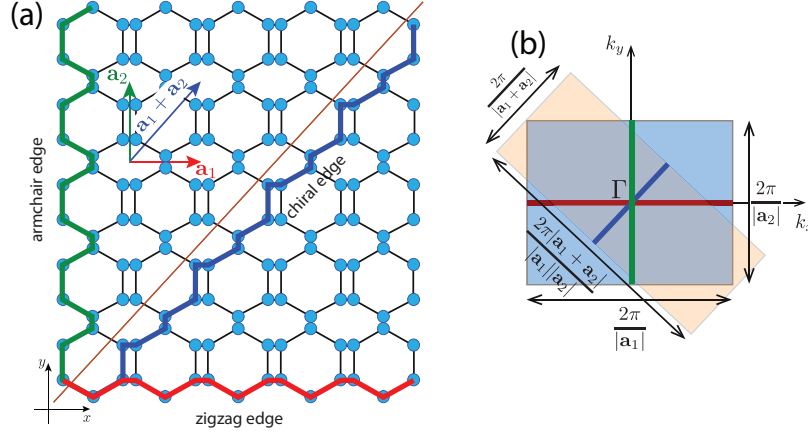


Fig. 2. (a) Schematic of edge structures for BPN PhC. The red line indicates the zigzag edge, whose translational vector is  $\mathbf{T} = \mathbf{a}_1$ . The armchair edge is expressed as the green line with translational vector  $\mathbf{T} = \mathbf{a}_2$ . The blue line denotes the chiral edge, whose translational vector is  $\mathbf{T} = \mathbf{a}_1 + \mathbf{a}_2$ . (b) The momentum areas used for calculation of Zak phase of BPN PhC with edges. The blue rectangle is momentum area used for the calculation of Zak phase for the ribbons with the zigzag and armchair edges. The orange rectangle is the momentum area used for the calculation of Zak phase for the ribbons with chiral edges. The size of each momentum area is written in black text. The red, green and blue bold lines are the 1st BZs of ribbons with the zigzag, armchair and chiral edges, respectively.

conditions: PBC for  $y$ -direction and PMC boundary condition for  $x$ -direction, respectively. Figure 3(f) is the corresponding photonic band structure for BPN ribbon with armchair edges. The numerically obtained Zak phase for BPN ribbon with armchair edges is shown in Fig. 3(e). The 1st and the 3rd photonic bands lead to nontrivial Zak phase with  $\pi$ , however, the 2nd photonic bands lead to Zak phase with 0. Thus, the total Zak phase for the lowest three bands is  $\sum_{n=1}^3 Z^n(k) = 2\pi$ , which is equivalent to 0. Therefore, the complete band gap between the 3rd and the 4th photonic band becomes topologically trivial. As can be seen in Fig. 3(f), there is no topological edge state in the complete band gap between the 3rd and the 4th photonic bands, which is consistent with the Zak phase calculation. Similar to BPN ribbon with zigzag edges, topological edge states should appear in the photonic band gaps between the 1st and the 2nd bands, and also between the 2nd and the 3rd bands. However, because of the overlapping frequency of these two pairs of band, we cannot distinguish the topological edge states from bulk states by numerical calculation.

Finally, we shall consider the case for BPN ribbon with chiral edges shown in Fig. 3(g). As for BPN ribbon with chiral edges, translational invariance is preserved along the direction of  $\mathbf{T} = \mathbf{a}_1 + \mathbf{a}_2$  and its width in  $x$ -direction is  $20a_0$ . Figure 3(i) shows the corresponding photonic band structure for BPN ribbon with chiral edges, in which the blue lines indicate the modes owing to topological edge states. In numerical calculation, we shall take the following boundary conditions: PBC for the translational invariant direction and PMC boundary condition for the transverse direction, respectively. Figure 3(h) shows the numerically obtained Zak phase for the lowest three photonic bands of BPN ribbon with chiral edges. Although the Zak phase for the lowest two photonic bands are 0, it is  $\pi$  for the 3rd band. The complete band gap becomes topologically nontrivial because the total Zak phase of the lowest three photonic bands is  $\sum_{n=1}^3 Z^n(k) = \pi$ . Since the photonic band gap between the 3rd and the 4th photonic bands

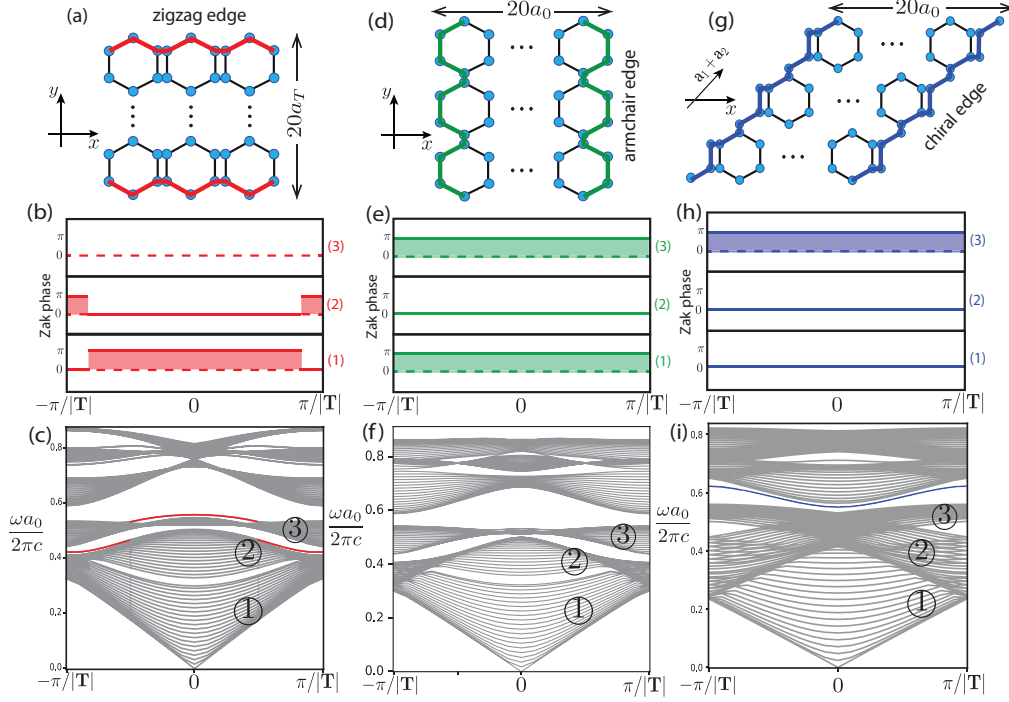


Fig. 3. (a) Schematic structure of a ribbon with zigzag edges, where the  $x$ -direction is periodic but the  $y$ -direction is finite with the width  $20a_T$ . (b) The Zak phase of the lowest three bands of BPN PhC with zigzag edges. (c) Photonic band structure for BPN ribbon with zigzag edges. The red lines indicate topological edge states. (d) Schematic of BPN PhC ribbon with armchair edges, which is periodic along  $y$ -direction and finite in  $x$ -direction. Its size in  $x$ -direction is  $20a_0$ . (e) The Zak phase of the lowest three bands of BPN PhC ribbon with armchair edges. (f) Photonic band structure for BPN PhC ribbon with armchair edges. (g) Schematic of BPN PhC ribbon with chiral edges, which is periodic along  $\mathbf{T} = \mathbf{a}_1 + \mathbf{a}_2$  direction and finite in  $x$ -direction. This ribbon's width is also  $20a_0$  in  $x$ -direction. (h) The Zak phase of the lowest three bands of BPN PhC in  $\mathbf{T} = \mathbf{a}_1 + \mathbf{a}_2$  direction. (i) Photonic band structure for BPN PhC ribbon with chiral edges. The blue lines indicate topological edge states.

are topological, the topological edge states emerge as shown in Fig. 3(i).

To confirm the existence of topological zigzag edge states at all  $k$  points, we create another structure containing BPN PhC and a trivial PhC. The trivial PhC has a band gap at the same frequency range as the band gap of BPN PhC. Figure 4(a) is the schematic of a supercell containing 10 unit cells of BPN PhC and 10 unit cells of trivial PhC in the  $y$ -direction. This structure has the interface between the zigzag edge and the trivial PhC. Applying the PBC in both  $x$ - and  $y$ -directions, we calculate and obtain the photonic band structure for the supercell as shown in Fig. 4(b). The red lines denote topological edge states, where the EM wave is localized at the interfaces. These edge states emerge at all  $k$  points in the 1st BZ and doubly degenerate because the supercell contains two interfaces.

We have examined three different types of ribbon structures of BPN PhC. At the complete band gap between bands 3 and 4, the armchair ribbon is topologically trivial, the zigzag and chiral ribbons are topologically nontrivial resulting in the emergence of topological edge states. All the topological edge states are doubly degenerate because each supercell has two equivalent boundaries.

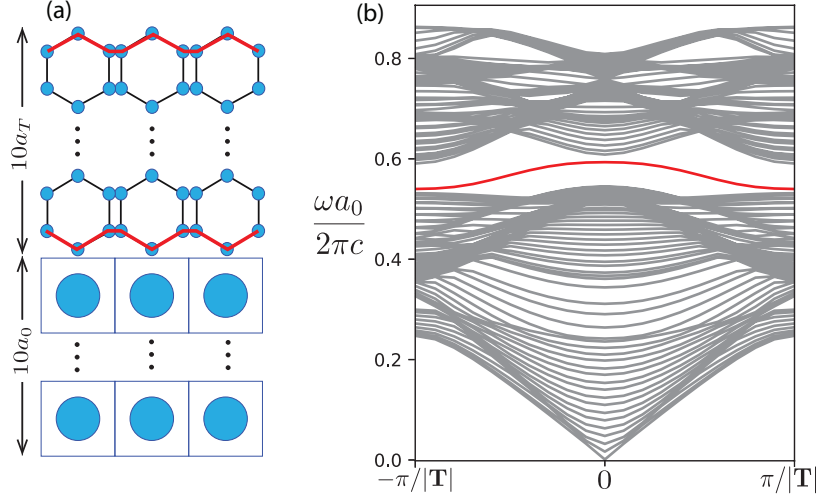


Fig. 4. (a) Schematic of a structure including 10 BPN PhC unit cells and 10 trivial PhC unit cells in  $y$ -direction. This structure is periodic in both  $x$ - and  $y$ -directions and contains the interface between BPN ribbon with zigzag edges and the trivial PhC. (b) The corresponding photonic band structure for the structure of (a). The red lines denote topological edge states, where EM wave is highly localized at the interface between the zigzag edge and the trivial PhC.

#### 4. Topological Corner States

The topological corner states, as a manifestation of higher-order topology, are examined. These states involve the confinement of EM waves at the corner owing to the non-zero product of the Zak phase in two edge directions forming the corner structure [20, 40, 43]. In this section, we examine the localization of EM waves at different corner structures in the BPN PhC lattice.

In Fig. 5(a), we show a rhombus-shaped BPN PhC. Four outer boundaries have the chiral edges. Since there are two possible ways to construct a rhombus-shaped BPN PhC with chiral edges, to distinguish this rhombus structure with the latter one, we refer to as "type I". The two opposite corners have the same structure and they are different from two other ones. The PMC boundary condition is applied for all edges in this rhombus structure. Figure 5(b) is the frequency spectrum for the type I rhombus-shaped BPN PhC. In the complete band gap of BPN PhC, there are four isolated states labeled by red stars. These states are corner states where the EM wave is highly localized at the corners and exponentially decays as shown in Fig. 5(c). Since the corner structure are formed by the two chiral edges which are topological, the product of Zak phases among these two chiral edges gives nonzero Zak phase  $\pi$ . Thus, the corner state are topologically protected states, because the topological corner states based on the same condition are observed in other topological systems [20, 40].

Similarly, we can construct another corner structure from two chiral edges, which we refer to as "type II" as shown in Fig. 6(a). The difference of type II structure from type I can be seen at the corner sites. Figure 6(b) shows the frequency spectrum for type II, where four isolated states labeled by red stars are numerically observed in the complete band gap. These states are also topological corner states according to the same reason of type I. Their EM waves distribute mainly at the corners, and decay exponentially as shown in Fig. 6(c), in which the frequency increases from left to right panels.

Finally, we examine another corner structure which is formed by the zigzag and the chiral edges as shown in Fig. 7(a). The left and right are chiral edges, the upper and lower are zigzag



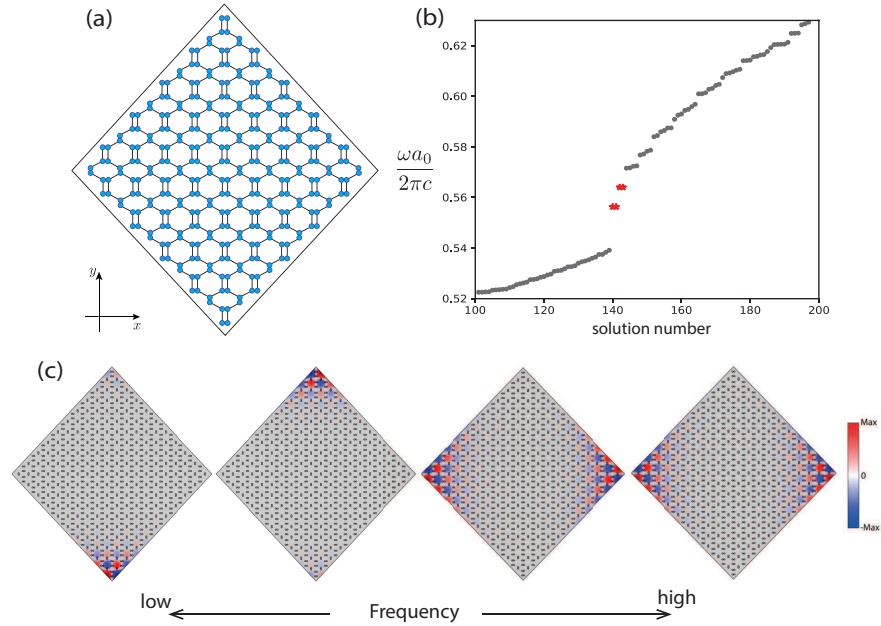


Fig. 5. (a) Schematic of corner structure which is formed by chiral edges (type I). (b) Frequency spectrum for type I. The red stars indicate topological corner states. The frequency range of corner states is in the complete gap region. (c) The field profile for four corner states from low to high frequencies. These profiles show that topological corner states is isolated from bulk and edge states.

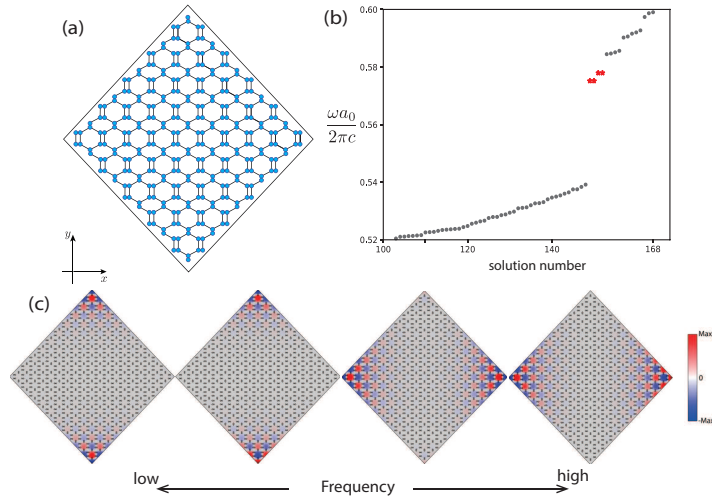


Fig. 6. (a) Schematic of corner structure of type II. Edges are chiral edges same as type I, however, the detail structures around corner are different. (b) Frequency spectrum for type II. The red stars indicate topological corner states. The frequency range of corner states is in the complete gap region. (c) The field profile for four corner states from low to high frequencies. These profiles show that topological corner states is isolated from bulk and edge states.

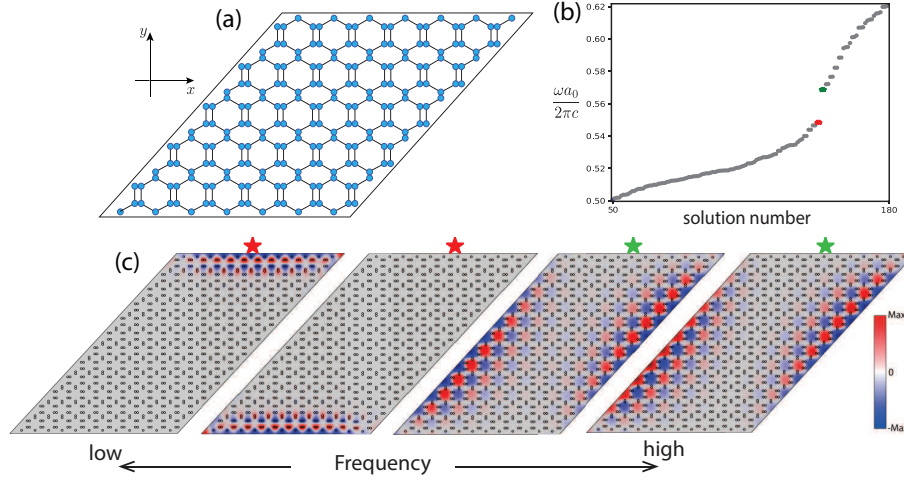


Fig. 7. (a) Schematic of corner structure formed by zigzag and chiral edges. (b) Photonic band structure for the corner structure formed by the zigzag and the chiral edges. The red stars indicate the zigzag edge states, the green stars denote the edge states of chiral edge. (c) The field distribution for the states labeled in red and green from low to high frequencies.

edges. Because both the zigzag and chiral edges are topologically nontrivial at the complete band gap, the topological corner states are expected to emerge in this structure. Figure 7(b) displays photonic band structure for the corner structure containing zigzag and chiral edges. The states below the band gap (labeled with red stars) represent the edge states at the zigzag edges, while the states above the band gap (labeled with green stars) correspond to the edge states at the chiral edges. Their field distributions are shown in Fig. 7(c), where the frequency increases from left to right panels. This frequency range is consistent with the frequency range of the edge states for the BPN edges with zigzag edges and BPN edges with chiral edges, as shown in Fig. 3(f) and (i), respectively. However, no corner states are found in this structure.

When we refer to existing research on 2D crystal structures where topological corner states emerge [20,40,48,56], we find that the two edges forming the corner are topologically nontrivial, and their frequency levels are identical. This allows them to interact with each other to form topological corner states. The reason for the absence of topological states in the present structure is that the frequency ranges of the zigzag and chiral edge states are entirely different, preventing any interaction between the two edge states. Therefore, electromagnetic waves cannot be confined to the boundary between two edges.

Other corner structures involving the armchair edge, such as corners between the zigzag and armchair edges or corners between the armchair and the chiral edges, can also be constructed. However, topological corner states do not exist in these structures due to the trivial properties within the complete band gap of the armchair edge.

## 5. Summary

In this paper, we have numerically studied EM waves in BPN PhC structure by using finite difference and finite element methods. The original photonic analog of the BPN has no band gap. Linear dispersion of frequency can be observed in this PhC. When the structure is modified by increasing the distance from each rod to the center of the unit cell, a complete band gap opens in between the 3rd and the 4th photonic bands. We examine the topological properties of BPN PhC in this photonic band gap by numerically calculating the Zak phase for several different

edge structures. The topological edge states are observed in the photonic band gap due to the nontrivial Zak phase, which are localized at the zigzag and the chiral edges. The higher-order topology as the corner states are found at the corner formed by two chiral edges because of non-zero product of the Zak phase in two directions. We also point out that the topological corner states emerge only when the topological edge states of two edge structures which form the corner are completely overlapped to each other.

Compared with graphene-like PhCs, the topological edge states in BPN-like structures can be found without breaking the symmetry of the crystals. Our results suggest a possible way to design in-gap topological waveguide and topological confinement of EM waves.

**Funding.** Japan Society for the Promotion of Science (22H05473, 21H01019, JP18H01154); Japan Science and Technology Agency (JPMJCR19T1).

**Acknowledgments.** K.W. acknowledges the financial support by JSPS KAKENHI (Grant No. 22H05473, 21H01019 and JP18H01154), and JST CREST (Grant No. JPMJCR19T1).

**Disclosures.** The authors declare no conflicts of interest.

**Data Availability Statement.** Data underlying the results presented in this paper are not publicly available at this time but may be obtained from the authors upon reasonable request.

## References

1. A. Bansil, H. Lin, and T. Das, “*Colloquium* : Topological band theory,” *Rev. Mod. Phys.* **88**, 021004 (2016).
2. M. Z. Hasan and C. L. Kane, “*Colloquium* : Topological insulators,” *Rev. Mod. Phys.* **82**, 3045–3067 (2010).
3. X.-L. Qi and S.-C. Zhang, “Topological insulators and superconductors,” *Rev. Mod. Phys.* **83**, 1057–1110 (2011).
4. Y. Ando, “Topological insulator materials,” *J. Phys. Soc. Jpn.* **82**, 102001 (2013).
5. M. Sato and S. Fujimoto, “Majorana fermions and topology in superconductors,” *J. Phys. Soc. Jpn* **85**, 072001 (2016).
6. D. Kong, J. C. Randel, H. Peng, J. J. Cha, S. Meister, K. Lai, Y. Chen, Z.-X. Shen, H. C. Manoharan, and Y. Cui, “Topological insulator nanowires and nanoribbons,” *Nano Lett.* **10**, 329–333 (2010). PMID: 20030392.
7. B. A. Bernevig, T. L. Hughes, and S.-C. Zhang, “Quantum spin hall effect and topological phase transition in hgte quantum wells,” *Science* **314**, 1757–1761 (2006).
8. M. Kim, J. Kim, Y. Hou, D. Yu, Y.-J. Doh, B. Kim, K. W. Kim, and J. Suh, “Nanomechanical characterization of quantum interference in a topological insulator nanowire,” *Nat. Commun.* **10**, 4522 (2019).
9. L. Fu, C. L. Kane, and E. J. Mele, “Topological insulators in three dimensions,” *Phys. Rev. Lett.* **98**, 106803 (2007).
10. C. L. Kane and E. J. Mele, “Quantum spin hall effect in graphene,” *Phys. Rev. Lett.* **95**, 226801 (2005).
11. Y. L. Chen, J. G. Analytis, J.-H. Chu, Z. K. Liu, S.-K. Mo, X. L. Qi, H. J. Zhang, D. H. Lu, X. Dai, Z. Fang, S. C. Zhang, I. R. Fisher, Z. Hussain, and Z.-X. Shen, “Experimental realization of a three-dimensional topological insulator,  $\text{Bi}_2\text{Te}_3$ ,” *Science* **325**, 178–181 (2009).
12. R. Okuyama, W. Izumida, and M. Eto, “Topological classification of the single-wall carbon nanotube,” *Phys. Rev. B* **99**, 115409 (2019).
13. P. Delplace, D. Ullmo, and G. Montambaux, “Zak phase and the existence of edge states in graphene,” *Phys. Rev. B* **84**, 195452 (2011).
14. D. Obana, F. Liu, and K. Wakabayashi, “Topological edge states in the su-schrieffer-heeger model,” *Phys. Rev. B* **100**, 075437 (2019).
15. A. Yoshida, Y. Otaki, R. Otaki, and T. Fukui, “Edge states, corner states, and flat bands in a two-dimensional  $\mathcal{PT}$ -symmetric system,” *Phys. Rev. B* **100**, 125125 (2019).
16. Z.-D. Song, L. Elcoro, and B. A. Bernevig, “Twisted bulk-boundary correspondence of fragile topology,” *Science* **367**, 794–797 (2020).
17. K. Wakabayashi, Y. Takane, M. Yamamoto, and M. Sigrist, “Edge effect on electronic transport properties of graphene nanoribbons and presence of perfectly conducting channel,” *Carbon* **47**, 124 – 137 (2009).
18. Z. Song, Z. Fang, and C. Fang, “ $(d - 2)$ -dimensional edge states of rotation symmetry protected topological states,” *Phys. Rev. Lett.* **119**, 246402 (2017).
19. W. A. Benalcazar, B. A. Bernevig, and T. L. Hughes, “Quantized electric multipole insulators,” *Science* **357**, 61–66 (2017).
20. F. Liu and K. Wakabayashi, “Higher-order topology and fractional charge in monolayer graphene,” *Phys. Rev. Res.* **3**, 023121 (2021).
21. C.-M. Miao, Q.-F. Sun, and Y.-T. Zhang, “Second-order topological corner states in zigzag graphene nanoflake with different types of edge magnetic configurations,” *Phys. Rev. B* **106**, 165422 (2022).
22. G. Harari, M. A. Bandres, Y. Lumer, M. C. Rechtsman, Y. D. Chong, M. Khajavikhan, D. N. Christodoulides, and M. Segev, “Topological insulator laser: Theory,” *Science* **359** (2018).

23. Y. Wu, H. Liu, J. Liu, H. Jiang, and X. C. Xie, "Double-frequency Aharonov-Bohm effect and non-Abelian braiding properties of Jackiw-Rebbi zero-mode," *Natl. Sci. Rev.* **7**, 572–578 (2019).
24. W. Zhang, X. Xie, H. Hao, J. Dang, S. Xiao, S. Shi, H. Ni, Z. Niu, C. Wang, K. Jin, X. Zhang, and X. Xu, "Low-threshold topological nanolasers based on the second-order corner state," *Light Sci. Appl.* **9**, 109 (2020).
25. Y. Wu, H. Jiang, J. Liu, H. Liu, and X. C. Xie, "Non-abelian braiding of dirac fermionic modes using topological corner states in higher-order topological insulator," *Phys. Rev. Lett.* **125**, 036801 (2020).
26. M. He, H. Sun, and Q. L. He, "Topological insulator: Spintronics and quantum computations," *Front. Phys.* **14**, 43401 (2019).
27. F. D. M. Haldane and S. Raghu, "Possible realization of directional optical waveguides in photonic crystals with broken time-reversal symmetry," *Phys. Rev. Lett.* **100**, 013904 (2008).
28. S. Raghu and F. D. M. Haldane, "Analogues of quantum-hall-effect edge states in photonic crystals," *Phys. Rev. A* **78**, 033834 (2008).
29. Z. Wang, Y. D. Chong, J. D. Joannopoulos, and M. Soljacic, "Reflection-free one-way edge modes in a gyromagnetic photonic crystal," *Phys. Rev. Lett.* **100**, 013905 (2008).
30. Z. Wang, Y. Chong, J. D. Joannopoulos, and M. Soljacic, "Observation of unidirectional backscattering-immune topological electromagnetic states," *Nature* **461**, 772–5 (2009).
31. M. Hafezi, E. A. Demler, M. D. Lukin, and J. M. Taylor, "Robust optical delay lines with topological protection," *Nat. Phys.* **7**, 907–912 (2011).
32. A. B. Khanikaev, S. H. Mousavi, W.-K. Tse, M. Kargarian, A. H. MacDonald, and G. Shvets, "Photonic topological insulators," *Nat. Mater.* **12**, 233–9 (2013).
33. M. Hafezi, S. Mittal, J. Fan, A. Migdall, and J. M. Taylor, "Imaging topological edge states in silicon photonics," *Nat. Photon.* **7**, 1001–1005 (2013).
34. M. C. Rechtsman, J. M. Zeuner, Y. Plotnik, Y. Lumer, D. Podolsky, F. Dreisow, S. Nolte, M. Segev, and A. Szameit, "Photonic floquet topological insulators," *Nature* **496**, 196–200 (2013).
35. S. A. Skirlo, L. Lu, and M. Soljacic, "Multimode One-Way Waveguides of Large Chern Numbers," *Phys. Rev. Lett.* **113**, 113904 (2014).
36. H. Cheng, L. Lin, X.-C. Sun, X.-P. Liu, M.-H. Lu, and Y.-F. Chen, "Topological photonic states," *Int. J. Mod Phys B* **28**, 1441001 (2014).
37. M. Blanco de Paz, C. Devescovi, G. Giedke, J. J. Saenz, M. G. Vergniory, B. Bradlyn, D. Bercioux, and A. García-Etxarri, "Tutorial: Computing topological invariants in 2d photonic crystals," *Adv. Quantum Technol.* **3**, 1900117 (2020).
38. F. Liu, H.-Y. Deng, and K. Wakabayashi, "Topological photonic crystals with zero berry curvature," *Phys. Rev. B* **97**, 035442 (2018).
39. X.-D. Chen, W.-M. Deng, F.-L. Shi, F.-L. Zhao, M. Chen, and J.-W. Dong, "Direct observation of corner states in second-order topological photonic crystal slabs," *Phys. Rev. Lett.* **122**, 233902 (2019).
40. Y. Ota, F. Liu, R. Katsumi, K. Watanabe, K. Wakabayashi, Y. Arakawa, and S. Iwamoto, "Photonic crystal nanocavity based on a topological corner state," *Optica* **6**, 786–789 (2019).
41. Y.-H. He, Y.-F. Gao, H.-Z. Lin, M.-C. Jin, Y. He, and X.-F. Qi, "Topological edge and corner states based on the transformation and combination of photonic crystals with square lattice," *Opt. Commun.* **512**, 128038 (2022).
42. X.-D. Chen, D. Zhao, X.-S. Zhu, F.-L. Shi, H. Liu, J.-C. Lu, M. Chen, and J.-W. Dong, "Edge states in self-complementary checkerboard photonic crystals: Zak phase, surface impedance, and experimental verification," *Phys. Rev. A* **97**, 013831 (2018).
43. F. Liu, H.-Y. Deng, and K. Wakabayashi, "Helical topological edge states in a quadrupole phase," *Phys. Rev. Lett.* **122**, 086804 (2019).
44. H. Xue, Y. Yang, G. Liu, F. Gao, Y. Chong, and B. Zhang, "Realization of an acoustic third-order topological insulator," *Phys. Rev. Lett.* **122**, 244301 (2019).
45. H.-X. Wang, L. Liang, B. Jiang, J. Hu, X. Lu, and J.-H. Jiang, "Higher-order topological phases in tunable c3 symmetric photonic crystals," *Photon. Res.* **9**, 1854–1864 (2021).
46. X. Zhang, L. Liu, M.-H. Lu, and Y.-F. Chen, "Valley-selective topological corner states in sonic crystals," *Phys. Rev. Lett.* **126**, 156401 (2021).
47. S. Shao, L. Liang, J.-H. Hu, Y. Poo, and H.-X. Wang, "Topological edge and corner states in honeycomb-kagome photonic crystals," *Opt. Express* **31**, 17695–17708 (2023).
48. H. T. Phan, F. Liu, and K. Wakabayashi, "Valley-dependent corner states in honeycomb photonic crystals without inversion symmetry," *Opt. Express* **29**, 18277–18290 (2021).
49. Y. Shimomura, Y. Takane, and K. Wakabayashi, "Electronic states and local density of states in graphene with a corner edge structure," *J. Phys. Soc. Jpn.* **80**, 054710 (2011).
50. Q. Fan, L. Yan, M. W. Tripp, O. Krejčí, S. Dimosthenous, S. R. Kachel, M. Chen, A. S. Foster, U. Koert, P. Liljeroth, and J. M. Gottfried, "Biphenylene network: A nonbenzenoid carbon allotrope," *Science* **372**, 852–856 (2021).
51. A. Bafekry, M. Faraji, M. M. Fadlallah, H. R. Jappor, S. Karbasizadeh, M. Ghergherehchi, and D. Gogova, "Biphenylene monolayer as a two-dimensional nonbenzenoid carbon allotrope: a first-principles study," *J. Physics: Condens. Matter* **34**, 015001 (2021).
52. M.-C. Jin, Y.-F. Gao, H.-Z. Lin, Y.-H. He, and M.-Y. Chen, "Corner states in second-order two-dimensional topological photonic crystals with reversed materials," *Phys. Rev. A* **106**, 013510 (2022).

53. B.-Y. Xie, H.-F. Wang, H.-X. Wang, X.-Y. Zhu, J.-H. Jiang, M.-H. Lu, and Y.-F. Chen, "Second-order photonic topological insulator with corner states," *Phys. Rev. B* **98**, 205147 (2018).
54. J. Zak, "Berry's phase for energy bands in solids," *Phys. Rev. Lett.* **62**, 2747–2750 (1989).
55. H.-X. Wang, G.-Y. Guo, and J.-H. Jiang, "Band topology in classical waves: Wilson-loop approach to topological numbers and fragile topology," *New J. Phys.* **21**, 093029 (2019).
56. M. Li, D. Zhirihin, M. Gorlach, X. Ni, D. Filonov, A. Slobozhanyuk, A. Alù, and A. B. Khanikaev, "Higher-order topological states in photonic kagome crystals with long-range interactions," *Nat. Photonics* **14**, 89–94 (2020).